Journal of ELECTRONIC MATERIALS
DOI: 10.1007/s11664-011-1858-8


# Calculation of Nonlinear Thermoelectric Coefficients of $InAs_{1-x}Sb_x$ Using Monte Carlo Method

RAMIN BANAN SADEGHIAN,[1] JE-HYEONG BAHK,[1] ZHIXI BIAN,[1] and ALI SHAKOURI[1,2,3]

1.—Baskin School of Engineering, University of California, Santa Cruz, CA 95064, USA. 2.—School of Electrical and Computer Engineering, Purdue University, Electrical Engineering Building, 465 Northwestern Ave., West Lafayette, IN 47907-2035, USA. 3.—e-mail: shakouri@purdue.edu.

It was found that the nonlinear Peltier effect could take place and increase the cooling power density when a lightly doped thermoelectric material is under a large electrical field. This effect is due to the Seebeck coefficient enhancement from an electron distribution far from equilibrium. In the nonequilibrium transport regime, the solution of the Boltzmann transport equation in the relaxation-time approximation ceases to apply. The Monte Carlo method, on the other hand, proves to be a capable tool for simulation of semiconductor devices at small scales as well as thermoelectric effects with local nonequilibrium charge distribution. $InAs_{1-x}Sb_x$ is a favorable thermoelectric material for nonlinear operation owing to its high mobility inherited from the binary compounds InSb and InAs. In this work we report simulation results on the nonlinear Peltier power of $InAs_{1-x}Sb_x$ at low doping levels, at room temperature and at low temperatures. The thermoelectric power factor in nonlinear operation is compared with the maximum value that can be achieved with optimal doping in the linear transport regime.

**Key words:** Nonlinear Peltier coefficient, InAsSb, Monte Carlo simulation

## INTRODUCTION

Contrary to the nonlinear current–voltage behavior, which is common in active electron devices, nonlinear thermoelectric effects have not been the subject of detailed studies. The Peltier coefficient, Π, for instance, is current independent at low applied electric fields, in the linear conduction regime. At elevated fields, Π may increase nonlinearly with field, making it beneficial for high-efficiency thermoelectric cooling applications.

Nonlinear thermoelectric effects in metallic films and InGaAs were demonstrated earlier.[1–3] Among all the III–V semiconductors, $InAs_{1-x}Sb_x$ has the smallest band gap, with values about 0.1 eV at room temperature.[4,5] This, along with its high mobility, makes InAsSb a desirable material for mid-infrared optoelectronic devices, including lasers and photodetectors. In addition, its high electron mobility, inherent to the binary compounds InSb and InAs, is also favorable for achieving a high thermoelectric power factor. The alloy composition can be selected so as to optimize the thermoelectric figure of merit. This work focuses on $InAs_{0.1}Sb_{0.9}$ and $InAs_{0.3}Sb_{0.7}$.

## MONTE CARLO SIMULATIONS

At low electric fields, where carrier transport is often interrupted by scattering events, the electron energy can be fully relaxed by scattering processes, forcing the electrons to cool down to lattice temperature. In this case, the Boltzmann transport equation (BTE) can be solved by employing the relaxation-time approximation where the transport coefficients happen to be independent of the electric field.[6,7] At high fields, however, as we approach the nonlinear transport regime, electrons can be sufficiently accelerated by the electric field before scattering events occur, so that the electron temperature begins to exceed the lattice temperature.

The following definition of the Peltier coefficient, Π, was implemented to extract the Seebeck coefficient, $S$,

(Received July 17, 2011; accepted December 5, 2011)

Published online: 28 December 2011

from the thermal, $J_Q$, and electrical, $J_e$, current densities, which were computed separately in our Monte Carlo code, while the lattice temperature was fixed at $T$:

$$ST = \Pi = \left.\frac{J_Q}{J_e}\right|_{\nabla T=0}. \quad (1)$$

Average values of electrical conductivity, $\sigma$, and mobility, $\mu_e$, were obtained at different current densities using the macroscopic relationship

$$\sigma = J_e/E \approx \mu_e n_e e, \quad (2)$$

where $E$ is the applied electric field, $n_e$ is the electron concentration, and $e$ is the electron charge. For simplicity reasons, a single-valley, nonparabolic band model for InAsSb was assumed. Table I presents the material parameters used in our Monte Carlo simulation. The device length was chosen to be $l$ = 0.5 $\mu$m (along the applied field direction), and the width, $w$, and height, $h$, were both 0.5 $\mu$m.

The code is three-dimensional in both position ($r$) and momentum ($k$) spaces, and employs contributions of alloy, intravalley polar optical phonon (POP), and impurity scattering mechanisms in modeling the electron conduction. The individual and total energy relaxation scattering rates of two doped $InAs_{0.1}Sb_{0.9}$ specimens as a function of electron energy are shown in Fig. 1. The scattering rates are calculated prior to execution of the main Monte Carlo loop. Figure 1a corresponds to $InAs_{0.1}Sb_{0.9}$ with total electron concentration of $n_e = 6.95 \times 10^{16}$ cm$^{-3}$, of which $5 \times 10^{16}$ cm$^{-3}$ ($0.72n_e$) is from impurity scatterers at 300 K, and Fig. 1b corresponds to the same composition at 200 K with $n_e = 1 \times 10^{16}$ cm$^{-3}$. The intrinsic carrier concentrations are $4 \times 10^{16}$ cm$^{-3}$ and $2.5 \times 10^{15}$ cm$^{-3}$ at 300 K and 200 K, respectively. The temperature dependence of impurity and POP scattering is discernible. Because of the temperature dependence of the electron energy distribution, the effect of alloy scattering also changes with

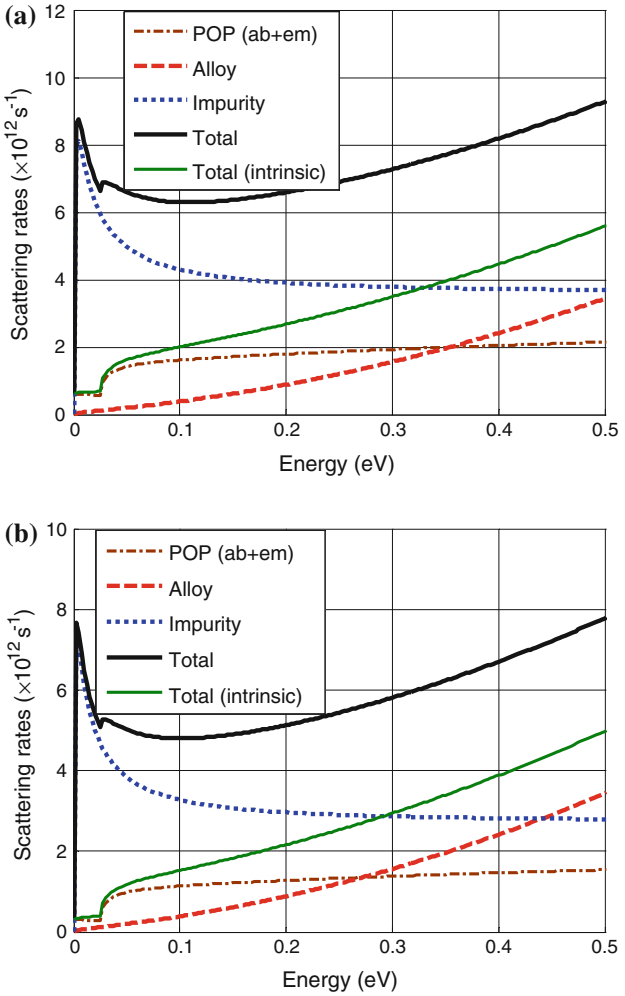


Fig. 1. Scattering rates of $InAs_{0.1}Sb_{0.9}$ at (a) 300 K with $n_e = 6.95 \times 10^{16}$ cm$^{-3}$ of which only $0.72n_e$ ($5.0 \times 10^{16}$ cm$^{-3}$) is from impurity dopants (impurity electron scatterers) and the rest from thermally excited electron-hole pairs, and at (b) 200 K with $n_e = 1 \times 10^{16}$ cm$^{-3}$. The total scattering rates of the undoped specimens are plotted for reference. POP rates include both absorption (ab) and emission (em) of optical phonons.

**Table I. Parameters for $InAs_{1-x}Sb_x$, from Refs. 4, 5, and 9**

| **Nonparabolicity, $\alpha$ (eV$^{-1}$)** | **Optical phonon energy, $\hbar\omega_0$ (eV)** | **Static dielectric constant, $\varepsilon_r\|_0$** | **High-frequency dielectric constant, $\varepsilon_r\|_\infty$** |
|---|---|---|---|
| $1.4(1-x) + 4.1x$ | 0.025 | $15.15 + 1.65x$ | $12.3 + 3.4x$ |

| **Density, $\rho$ (g cm$^{-3}$)** | **Alloy scattering potential, $U_{alloy}$ (eV)** | **Bowing factor, $E_g^\Gamma$ (eV)** | **Lattice thermal conductivity, $\kappa$ (W cm$^{-1}$ K$^{-1}$)** |
|---|---|---|---|
| $5.68 + 0.09x$ | 0.801 | 0.67 | $\left(\frac{x}{\kappa_{InSb}} + \frac{(1-x)}{\kappa_{InAs}} + 80x(1-x)\right)^{-1}$ |

temperature during the transport simulation within the Monte Carlo loop. Among the scattering mechanisms, only POP is inelastic and can limit the electron temperature, $T_{elec}$, directly. In addition, changes in the electron momentum distribution caused by the other two scattering mechanisms are reflected in the statistics of $T_{elec}$ and Fermi level, and in turn affect POP by the Pauli exclusion principle. Note that the heat equation is not solved and the lattice temperature and number of phonons are assumed to be fixed in our simulation. The simulation error due to this assumption will be small only when the device is operated with a small cooling/heating temperature. Furthermore, in the cooling performance estimation we have assumed that Joule heating is uniform in the bulk and the Peltier effect is localized at the boundaries, whose validity requires the device length to be much larger than the energy relaxation length, i.e., $l \gg l_i$. In this case, the maximum cooling, $\Delta T_{max}$, at a given applied electrical field, is achieved at an optimal film thickness, $l_{opt}$, calculated using

$$\Delta T_{max} = \frac{1}{2} Z T^2, \tag{3}$$

and

$$l_{opt} = ST\sigma/J, \tag{4}$$

respectively, where $T$ is the absolute (lattice) temperature, and $Z$ is the figure of merit defined as[8]

$$Z = \sigma S^2/(\kappa + \kappa_{elec}). \tag{5}$$

In Eq. 5, $\kappa$ and $\kappa_{elec}$ represent the lattice and electronic thermal conductivities, respectively, and $\sigma S^2$ is the so-called thermoelectric power factor. $\kappa$ was estimated using published thermal conductivity data for InAs and InSb at 300 K and 200 K,[5,9] assuming the bowing factor of thermal resistivity not to vary with temperature.[9] $\kappa_{elec}$ was calculated using the Wiedemann–Franz relationship given by $\kappa_{elec} = L\sigma T_{elec}$, in which $L = 2.44 \times 10^{-8}$ W Ω $K^{-2}$ was used. At low carrier densities, $L$ should be a smaller number, particularly in the linear regime, whereas it is an unknown quantity in the nonlinear regime. However, since in general $\kappa \gg \kappa_{elec}$ within the concentration ranges studied here ($\kappa_{elec} \approx 0.084\kappa$ at maximum with the above assumption), the resulting total thermal conductivity is still a good approximation. In the case that a fixed device length is assumed, the cooling temperature at a given current density can be calculated from the following heat balance equation:

$$JST - \frac{1}{2}\frac{J^2}{\sigma} l = \frac{\kappa}{l}\Delta T, \tag{6}$$

in which the Peltier cooling and Joule heating are balanced with the thermal conduction at steady state.

## RESULTS AND DISCUSSION

Curves of electron mobility and conductivity as a function of current density are plotted in Fig. 2a and b, respectively. Figure 2c shows curves of current density against applied electric field. Each data point in the plots from this point forward corresponds to a fixed applied electric field. The effect

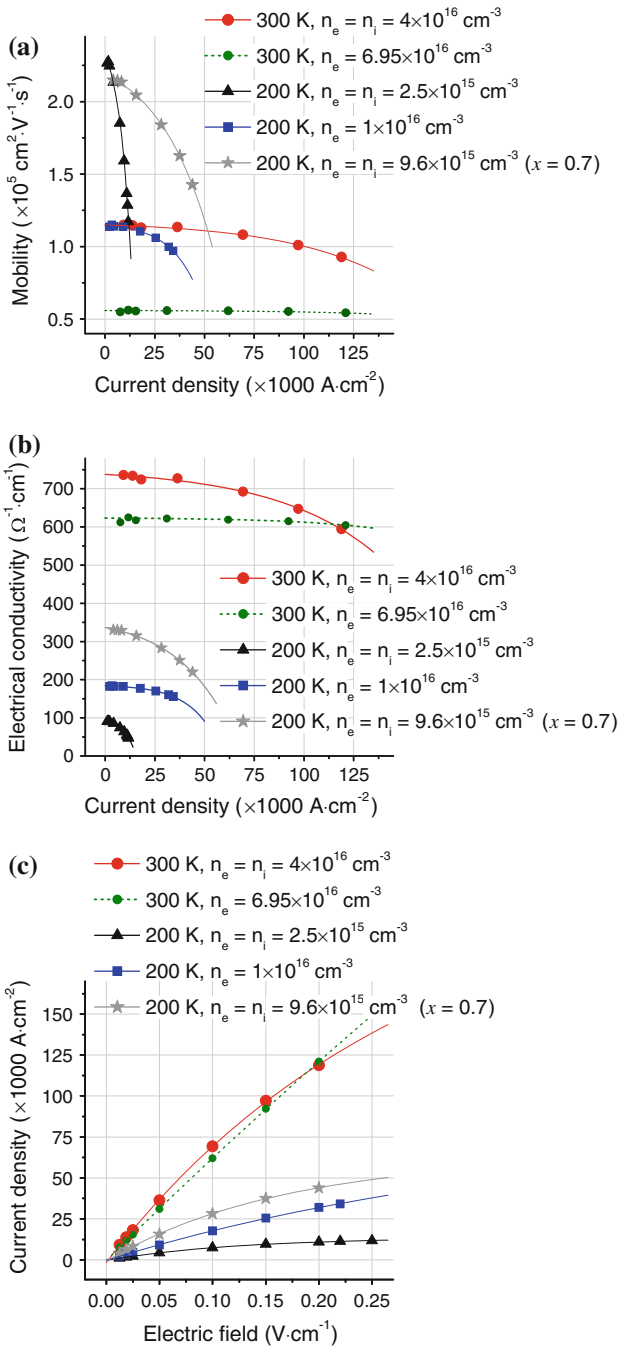


Fig. 2. Evolution of (a) electron mobility and (b) electrical conductivity, in $InAs_{0.1}Sb_{0.9}$ with current density at 300 K and 200 K. At 300 K, results were obtained for the intrinsic material (large circles, red in the online version) and the *n*-type doped material with total $n_e = 6.95 \times 10^{16}$ $cm^{-3}$ (small circles, green in the online version). At 200 K the curves are obtained for the intrinsic material with $n_i = 2.5 \times 10^{15}$ $cm^{-3}$ (triangles) and the *n*-type doped material with total $n_e = 1.0 \times 10^{16}$ $cm^{-3}$ (squares). The stars (gray) correspond to intrinsic $InAs_{0.3}Sb_{0.7}$ ($x = 0.7$) at 200 K, and the rest of the curves correspond to $x = 0.9$. (c) Current density as a function of applied electric field at different carrier densities and alloy compositions.

of impurity scattering as the dominant scattering mechanism on reducing the mobility is noticeable at both temperatures. At 300 K, although the mobility is adversely affected by impurity doping, the electrical conductivity is still close to that of the intrinsic material in both the linear and nonlinear transport regimes. At a given electric field, $InAs_{0.9}Sb_{0.1}$ displays a slightly larger mobility than $InAs_{0.7}Sb_{0.3}$ because of a smaller electron mass, as shown in Fig. 2a (200 K). However, the current densities are quite different because of a large contrast in the intrinsic carrier concentration. Notice the similarity of conductance characteristics in the undoped and doped materials at 300 K in Fig. 2c. At low temperatures, the degree of nonlinear (field-dependent) conduction increases dramatically because the total scattering rates decrease, the electron mean free path increases, and electrons are forced to accelerate significantly before their momentum is relaxed by scattering.

Monitoring the electronic temperature provides a means to indicate the transition point from linear to nonlinear operation. It is known that nonlinear operation starts when $T_{elec}$ begins to exceed the lattice temperature, $T$.[7] Figure 3 shows the evolution of $T_{elec}$ with current in all the cases studied. It is seen that such a transition occurs at relatively low biases and is pronounced at low temperatures. POP scattering is the only scattering mechanism that prevents unbounded growth of $T_{elec}$. The lattice temperature was kept constant in the simulation. Since phonon scattering is noticeably smaller at lower temperatures, $T_{elec}$ grows faster. Future work can incorporate lattice cooling/heating that allow changes in the phonon scattering for higher accuracy.

Curves of Peltier coefficient as a function of current density are shown in Fig. 4. Simulations showed that, at 300 K, intrinsic $InAs_{0.1}Sb_{0.9}$ is superior to the doped material with regard to the effective thermoelectric figure of merit in the nonlinear regime. To ascertain this, the coefficients of the intrinsic $InAs_{0.1}Sb_{0.9}$ (with intrinsic carrier concentration of $n_i = 4 \times 10^{16}$ cm$^{-3}$) are compared with those of an $n$-type doped semiconductor with total electron concentration of $n_e = 6.95 \times 10^{16}$ cm$^{-3}$, of which only $5 \times 10^{16}$ cm$^{-3}$ ($0.72n_e$) is from impurity dopants and the rest from thermal excitation of electron–hole pairs. In this case, BTE simulations show that the doped material displays a Peltier coefficient very close to that of the intrinsic semiconductor in the linear regime. However, at higher current densities as we approach the nonlinear regime, the doped material lags behind.

The threshold current density at which $\Pi$ becomes nonlinear is noticeably small even at room temperature compared with the values reported for other III–V semiconductor materials; for instance, nonlinearity starts at $1.5 \times 10^4$ A cm$^{-2}$ and $1.1 \times 10^3$ A cm$^{-2}$ in intrinsic $InAs_{0.1}Sb_{0.9}$ at 300 K and 200 K, respectively, whereas for InGaAs doped for maximum cooling at 77 K, the threshold current density is $1 \times 10^4$ A cm$^{-2}$.[3] This is indeed a major improvement over InGaAs. As shown in the curves of $J_e(E)$ in Fig. 2c, these currents are achievable at bias voltages as low as 0.025 V applied across a 5-$\mu$m-thick InAsSb device. In the linear regime, at 300 K, the Peltier coefficients and electrical conductivities of the intrinsic and the doped $InAs_{0.1}Sb_{0.9}$ with 72% of carriers originated from ionized impurities are close to each other. However, as the nonlinear regime is approached at high currents, the Peltier coefficient of the extrinsic material becomes smaller than that of the intrinsic material. Therefore, it can be concluded that impurity scattering adversely affects the nonlinear thermopower, and thus the intrinsic sample exhibits the maximum thermopower in both the linear and nonlinear regimes.

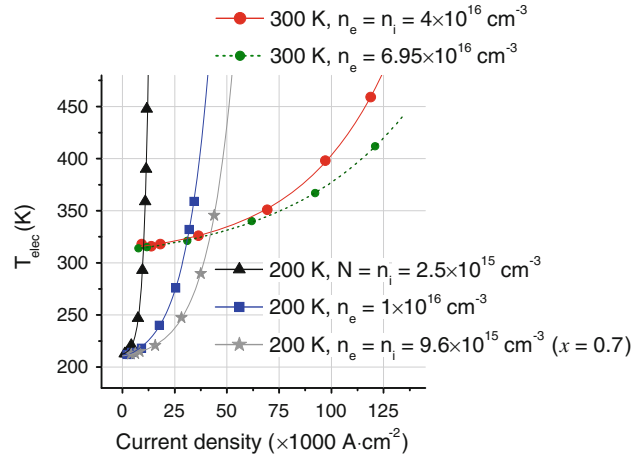


Fig. 3. Electron temperature as a function of current density for the carrier densities and alloy compositions described in Fig. 2.

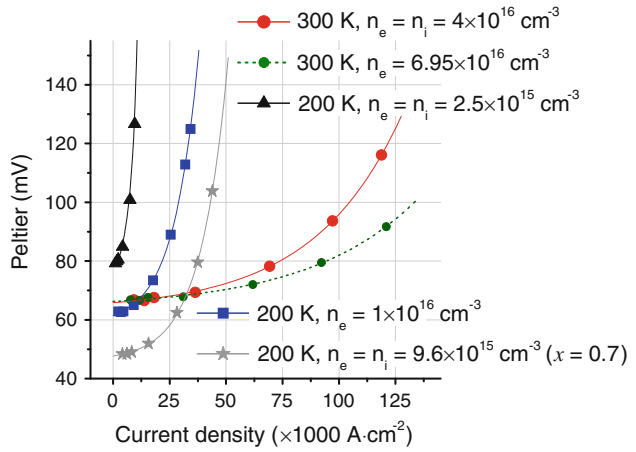


Fig. 4. Peltier coefficient as a function of current density for the carrier densities and alloy compositions described in Fig. 2. Note that the Peltier coefficient of the doped $InAs_{0.1}Sb_{0.9}$ at 300 K in the linear regime is close to that of the intrinsic material.

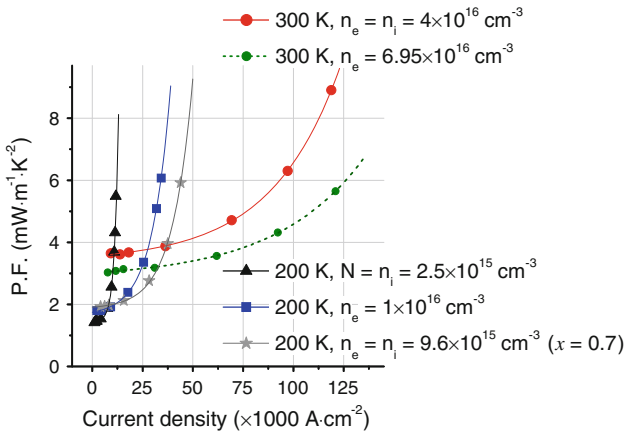


Fig. 5. Power factor as a function of current density for the carrier densities and alloy compositions described in Fig. 2.

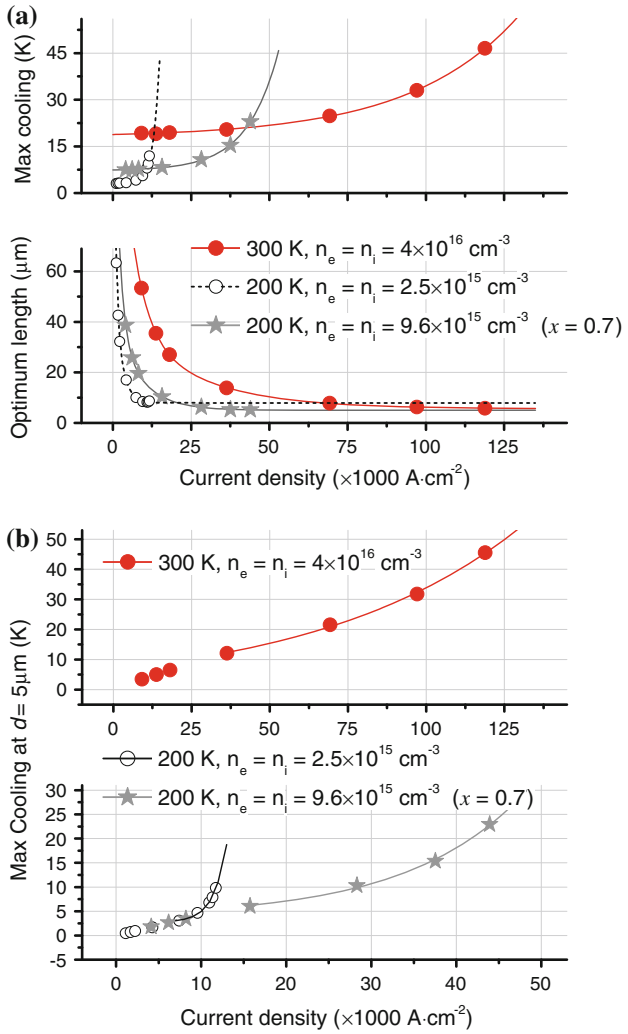


Fig. 6. Maximum cooling temperature as a function of current density: (a) calculated assuming optimum device length (also shown in the figure), and (b) at constant device length of $l = 5$ $\mu$m. Solid and hollow circles (red and black in the online version) represent intrinsic $InAs_{0.1}Sb_{0.9}$ at 300 K and 200 K, respectively, and the stars (grey) represents intrinsic $InAs_{0.3}Sb_{0.7}$ at 200 K. Linear and nonlinear regimes can be clearly distinguished.

Curves of power factor and maximum cooling against current density are plotted in Figs. 5 and 6, respectively. It is found that the intrinsic $InAs_{0.1}Sb_{0.9}$ exhibits the optimum power factor at both 300 K and 200 K because of the lack of ionized impurity scattering, and thus increased electron mobility. Note that, for intrinsic materials, hole transport is still negligible compared with the electron contribution due to the large mobility contrast of these two types of charge carrier. At 200 K the results are compared with those of $InAs_{0.3}Sb_{0.7}$, which has a smaller thermal conductivity. Because of its higher electrical conductivity (see Fig. 2b), $InAs_{0.3}Sb_{0.7}$ outperforms $InAs_{0.1}Sb_{0.9}$ at low current densities, but the Peltier coefficient of $InAs_{0.1}Sb_{0.9}$ increases more rapidly, and so does its power factor. The curves of maximum cooling temperature and optimum device length against current density were computed using Eqs. 3 and 4, and are shown in Fig. 6a. The cooling temperature of $InAs_{0.1}Sb_{0.9}$ is improved by 250% at room temperature. At high current densities, the optimum thickness for maximum cooling of $InAs_{0.1}Sb_{0.9}$ at 300 K approaches 5 $\mu$m, the value used in this simulation. Figure 6b shows plots of maximum cooling for fixed device length ($l = 5$ $\mu$m), calculated using Eq. 6. The linear and nonlinear parts are distinguishable. Although $InAs_{0.3}Sb_{0.7}$ has lower $\kappa$, and displays a higher power factor at low current densities, $InAs_{0.1}Sb_{0.9}$ performs better in the nonlinear regime at high current densities because of its much larger Peltier coefficient.

## CONCLUSIONS

Nonlinear thermoelectric coefficients of InAsSb were computed using a Monte Carlo scheme. It is shown that, at room temperature, in the nonlinear regime, maximum cooling of more than twice as much as in the linear regime can be achieved within the studied current density range. The intrinsic material outperforms the doped one. At 200 K, in the nonlinear regime, the rate of increase of the power factor with current becomes drastically higher than that at room temperature. $InAs_{0.3}Sb_{0.7}$ has a slightly better low-temperature cooling performance than $InAs_{0.1}Sb_{0.9}$ at low current densities because of its lower thermal conductivity and higher conductance, but the latter outperforms the former at high current densities.

## ACKNOWLEDGEMENTS

This work was partially funded by Advanced Research Projects Agency - Energy (ARPA-E) and Defense Advanced Research Projects Agency / Nano-Structured Materials for Power (DARPA/NMP).

## REFERENCES

1. I.O. Kulik, *J. Phys. Condens. Matter* 6, 9737 (1994).
2. A.N. Grigorenko, P.I. Nikitin, D.A. Jelski, and T.F. George, *J. Appl. Phys.* 69, 3375 (1991).
3. M. Zebarjadi, K. Esfarjani, and A. Shakouri, *Appl. Phys. Lett.* 91, 122104 (2007).
4. I. Vurgaftman, J.R. Meyer, and L.R. Ram-Mohan, *J. Appl. Phys.* 89, 5815 (2001).

5. *New Semiconductor Materials, Characteristics and Properties* (St. Petersburg: Ioffe Physico-Technical Institute, 1998–2001), http://www.ioffe.ru/SVA/NSM/Semicond/InAsSb/. Accessed 29 Nov 2011.
6. A. Shakouri and M. Zebarjadi, *Thermal Nanosystems and Nanomaterials*, ed. S. Volz (Berlin: Springer, 2009), pp. 225–299.
7. A. Shakouri, *Annu. Rev. Mater. Res.* 41, 399 (2011).
8. Z.X. Bian and A. Shakouri, *Appl. Phys. Lett.* 89, 212101 (2006).
9. M. Guden and J. Piprek, *Model. Simul. Mater. Sci. Eng.* 4, 349 (1996).